Comparison between spring network models and continuum constitutive laws: Application to the large deformation of a capsule in shear flow

T. Omori,[1,*] T. Ishikawa,[2] D. Barthès-Biesel,[3] A.-V. Salsac,[3] J. Walter,[3] Y. Imai,[2] and T. Yamaguchi[1]

[1]*Department of Biomedical Engineering, Tohoku University, Aoba 6-6-01 Sendai Miyagi, Japan*

[2]*Department of Bioengineering and Robotics, Tohoku University, Aoba 6-6-01 Sendai Miyagi, Japan*

[3]*Laboratoire de Biomécanique et Bioingénierie (UMR CNRS 6600), Université de Technologie de Compiègne, F-60205 Compiègne, France*

(Received 12 October 2010; revised manuscript received 24 January 2011; published 22 April 2011)

A capsule is a liquid drop enclosed by a solid, deformable membrane. To analyze the deformation of a capsule accurately, both the fluid mechanics of the internal and external fluids and the solid mechanics of the membrane must be solved precisely. Recently, many researchers have used discrete spring network models to express the membrane mechanics of capsules and biological cells. However, it is unclear whether such modeling is sufficiently accurate to solve for capsule deformation. This study examines the correlations between the mechanical properties of the discrete spring network model and continuum constitutive laws. We first compare uniaxial and isotropic deformations of a two-dimensional (2D) sheet, both analytically and numerically. The 2D sheet is discretized with four kinds of mesh to analyze the effect of the spring network configuration. We derive the relationships between the spring constant and continuum properties, such as the Young modulus, Poisson ratio, area dilation modulus, and shear modulus. It is found that the mechanical properties of spring networks are strongly dependent on the mesh configuration. We then calculate the deformation of a capsule under inflation and in a simple shear flow in the Stokes flow regime, using various membrane models. To achieve high accuracy in the flow calculation, a boundary-element method is used. Comparing the results between the different membrane models, we find that it is hard to express the area incompressibility observed in biological membranes using a simple spring network model.

DOI: 10.1103/PhysRevE.83.041918 PACS number(s): 87.16.D−, 47.63.−b, 46.15.−x, 83.80.Hj

I. INTRODUCTION

A capsule is a liquid drop enclosed by a solid, deformable membrane. Capsules are widely used in various fields, such as chemical engineering, biomedical engineering, and the food industry. They are usually suspended in another fluid. A viscous stress is exerted on the membrane owing to the motion of both the internal and external fluids. Understanding the deformation of capsules is important to predict their risk of rupture, either to prevent or favor it depending on the applications [1]. The capsule deformation is governed by fluid-structure interactions between the motion of the internal and external fluids and that of the capsule membrane. In particular, the discontinuity of the stress tensor across the thin membrane has to be taken into account. At the small scale of the capsule, the inertia forces of the internal and external flows are negligible compared to the viscous forces. The fluid velocity field is governed by the Stokes equations and can be evaluated in terms of surface integrals defined on the boundaries of the fluid domain, including the capsule membrane. This approach, known as the boundary-element method [2–4], treats the discontinuity of the stress tensor across the membrane explicitly; it is therefore one of the most accurate numerical methods to simulate a capsule in flow. Other methods, such as the immersed-boundary method, smooth out the stress tensor distribution over a thin domain [5–8] and are less accurate. In this study, we use a boundary-element method to solve the flow inside and outside the capsule to obtain high accuracy in the flow calculation.

The model chosen to solve the solid mechanics of the capsule membrane also plays a key role in the global accuracy of the simulation. The membrane thickness of a capsule is typically much smaller than the capsule size. In such a case, one may average the stress distribution across the thickness and assume the membrane to be a two-dimensional (2D) sheet. Several 2D constitutive laws have been proposed to model the mechanical behavior of a hyperelastic surface. For example, the 2D Mooney-Rivlin (MR) law has been used for isotropic volume-incompressible rubber-like materials. Area incompressible biological cell membranes are well modeled by the law introduced by Skalak *et al.* [9] (SK). It is now generally accepted that SK law can be extended to other types of hyperelastic materials, such as reticulated membranes that have low resistance to area dilation [10].

The dynamic response of a capsule (initially spherical, ellipsoidal or biconcave) has been extensively investigated for different membrane constitutive laws. The capsule deformation has been studied in various flow types, simple shear flow [2,5,6,11–14], Poiseuille tube flow [15–18], and elongational flow [19,20]. In some rare cases, the bending stiffness of the membrane has been taken into account [21]. These previous studies have clarified the influence of the membrane law on the capsule deformation.

Many researchers have used discrete spring network models to represent the membrane of capsules and biological cells. One of the main advantages of the spring network models is the simplicity of the mathematical description. One can avoid the numerical implementation of the complicated solid mechanics of the continuous models. In particular, spring network models have been used to model the membrane of red blood cells (RBC), which consists primarily of a phospholipid

*omori@pfsl.mech.tohoku.ac.jp

bilayer and an elastic spectrin network. From a mechanical point, the lipid bilayer strongly resists local area change, but the elasticity of the cytoskeleton enables the RBC to undergo large extensional deformation while maintaining the structural integrity of the membrane. Hansen *et al.* [22] have modeled the RBC membrane with an unstructured triangular network of identical linear springs. They have calculated the macroscopic elastic shear modulus and area expansion modulus of the model and showed that the mechanical properties of the spring network depend on the network configuration. Their study, however, was limited to small deformation. Navot [23] computed the strain energy of a spring network model and compared it to MR law.

Spring network models have been used also to model the motion of red blood cells in different flows such as 2D pore flow [24–26], 2D rouleaux dynamics [27], and tank-treading behavior of a discocyte [28]. However, it is unclear whether modeling the membrane with a spring network is sufficiently accurate to reproduce the complex behavior of capsules and cells. Furthermore, the values used for the spring models are often empirical and obtained for small deformation.

The objective of this paper is to investigate the influence of the membrane model on the dynamics of a capsule in flow. We thus compare a discrete spring network and different continuum membrane models in the domain of *large deformations* that are commonly encountered for capsules or cells. Different spring network configurations are considered that correspond to different meshing strategies for a capsule membrane. We first show how the spring constant must be adjusted so that a discrete spring model has the same small deformation elastic properties as a continuum model and investigate the effect of mesh resolution. We then show how the type of model used for the membrane affects the large deformation behavior of an initially spherical capsule in a simple shear flow.

II. MODELS FOR A 2D CAPSULE MEMBRANE

A. Continuum laws for a 2D hyperelastic material

When the thickness of a capsule membrane is small compared to the capsule dimensions and typical radius of curvature, the membrane can be modeled as a hyperelastic surface with negligible bending resistance and surface shear elastic modulus G_s, surface Young modulus E_s, surface Poisson ratio ν_s, and area dilatation modulus K_s. Of course, only two of those moduli are independent as they are related by the classical relations of elasticity

$$K_s = G_s \frac{1+\nu_s}{1-\nu_s}, \quad E_s = 2G_s(1+\nu_s), \tag{1}$$

For such an infinitely thin membrane, the principal components ε_1 and ε_2, of the Lagrange in-plane deformation tensor are related to the two principal extension ratios λ_1 and λ_2 by

$$\varepsilon_\alpha = \left(\lambda_\alpha^2 - 1\right)/2, \quad \alpha = 1,2. \tag{2}$$

Elastic stresses are replaced by elastic tensions that correspond to the forces per unit arc length measured in the plane of the membrane. When the membrane is isotropic in its plane, the principal directions of deformation and stress are colinear. A simple way to express the membrane constitutive law is thus to relate the two principal tensions T_1 and T_2 to the two principal extension ratios λ_1 and λ_2 (Fig. 1). The Young modulus E_s is obtained from a uniaxial stretching experiment, for example, in the x_1 direction $T_1 \neq 0, T_2 = 0$. In the limit of small deformation

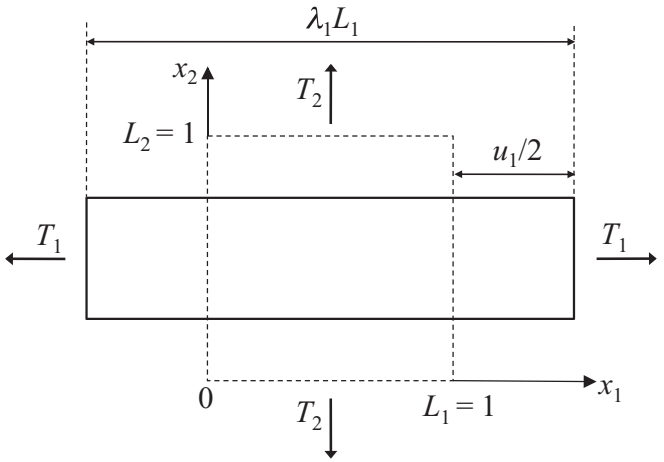

FIG. 1. Deformation of a 2D sheet along the principal axes. The broken and solid lines represent the reference and deformed states of the sheet, respectively. The deformation in the x_1 direction is defined by the stretch ratio λ_1 or by the displacement u_1 (with similar definitions in the x_2 direction). T_1 and T_2 are the tensions in the x_1 and x_2 directions, respectively.

$$T_1 = \frac{E_s}{2}\left(\lambda_1^2 - 1\right) = E_s \varepsilon_1. \tag{3}$$

The area dilation modulus K_s is obtained from isotropic stretching ($T_1 = T_2 = T$) and in the limit of small deformation is given by

$$T = K_s(\lambda_1\lambda_2 - 1) = K_s \Delta S/S, \tag{4}$$

where $\Delta S/S$ is the relative area change.

A number of laws are available to model thin hyperelastic membranes. Each law may model different material behaviors under large deformation. It is therefore possible to reproduce the strain softening of gelled membranes or the strain hardening of reticulated capsules with strong covalent links. For each law, we give only the expression for T_1 as a function of deformation. Tension T_2 may be found by inverting the indices 1 and 2. In the small deformation limit, all laws reduce to the 2D Hooke's law (H)

$$T_1^H = \frac{G_s}{1-\nu_s}\left[\lambda_1^2 - 1 + \nu_s\left(\lambda_2^2 - 1\right)\right], \tag{5}$$

where the surface Poisson ratio $\nu_s \in]-1, +1[$ is related to the area dilation modulus K_s according to Eq. (1). An area-incompressible membrane thus corresponds to $\nu_s \to 1$.

The 2D MR law describes the behavior of an infinitely thin sheet of a three-dimensional isotropic material that is volume incompressible

$$T_1^{\mathrm{MR}} = \frac{G_s^{\mathrm{MR}}}{\lambda_1\lambda_2}\left[\lambda_1^2 - \frac{1}{(\lambda_1\lambda_2)^2}\right]. \tag{6}$$

For small deformation, the correspondence between the material properties and the law parameters is

$$G_s = G_s^{\mathrm{MR}}, \quad E_s = 3G_s, \quad \nu_s = 1/2, \quad K_s = 3G_s. \tag{7}$$

The law (SK) derived by Skalak *et al.* [9] for 2D materials has independent surface shear and area dilation moduli

$$T_1^{\mathrm{SK}} = G_s^{\mathrm{SK}}\left[\frac{\lambda_1}{\lambda_2}\left(\lambda_1^2 - 1\right) + C\lambda_1\lambda_2\left(\lambda_1^2\lambda_2^2 - 1\right)\right]. \tag{8}$$

For small deformation, the correspondence between the material properties and the law parameters is

$$\begin{aligned} G_s &= G_s^{\mathrm{SK}}, \quad E_s = 2G_s\frac{2C+1}{C+1}, \\ \nu_s &= \frac{C}{C+1}, \quad K_s = G_s(1+2C). \end{aligned} \tag{9}$$

For large deformation, the condition $T_2 = 0$ provides an expression of λ_2 as a function of λ_1 that can be reported in Eqs. (5), (6), and (8) to provide the expression of the tension T_1 for the different constitutive laws. For large uniaxial deformation, the variation of T_1 with ε_1 is nonlinear. It can be shown that SK law is strain hardening, whereas MR law is strain softening [29].

B. Spring network model

We now consider a spring network to model the capsule membrane. A 2D sheet is discretized as a network of springs, with frictionless hinges at the nodal points. We assume that all the springs have the same elastic resistance proportional to the length change of the springs. Four kinds of mesh configuration are used in this study. Triangular meshes are often used to model the spectrin network of red blood cell membranes. We discuss the effect of mesh topology on the mechanical properties of the network.

1. Nodal forces

In general Cartesian coordinates, the spring force $\boldsymbol{f}_{ij}$ between two nodal points i and j is equal to

$$\boldsymbol{f}_{ij} = k(\|\boldsymbol{r}_{ij}\| - \|\boldsymbol{r}_{0,ij}\|)\frac{\boldsymbol{r}_{ij}}{\|\boldsymbol{r}_{ij}\|}, \quad \text{with} \quad \boldsymbol{f}_{ji} = -\boldsymbol{f}_{ij}, \tag{10}$$

where $\boldsymbol{r}_i$ and $\boldsymbol{r}_j$ are the position vectors of the nodal points i and j, $\boldsymbol{r}_{ij} = \boldsymbol{r}_j - \boldsymbol{r}_i$, and $\|\boldsymbol{r}_{0,ij}\|$ is the equilibrium length between nodes i and j. The spring constant is k.

2. Mesh configuration

A 2D sheet in the (x_1,x_2) plane has initial length L_1 and width L_2. It is discretized with four different meshes (Fig. 2). In the cross mesh (1), the membrane is discretized by squares with diagonal lines. This mesh is similar to the one used by Navot [23] to discuss correlations between the spring network model and MR law. In the cross-center mesh (2), nodal points are added at the intersections of the diagonal lines. In the regular-triangle mesh (3), the mesh is based on regular hexagons with a central node. An unstructured mesh (4) is created with the commercial mesh generator, GRIDGEN (ver. 15; Vinas Co., Ltd., Japan), based on the Delaunay triangulation algorithm.

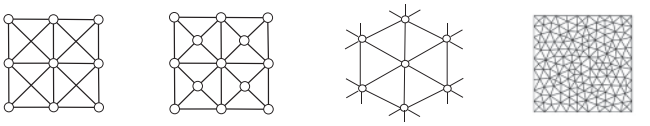

1. Cross 2. Cross Centre 3. Regular triangle 4. Unstructured

FIG. 2. The material is discretized by four types of mesh: cross, cross center, regular triangle, and unstructured.

The initial boundary grid spacings ΔL_1 and ΔL_2 are given by $\Delta L_1 = L_1/n$ and $\Delta L_2 = L_2/m$, where n and m are the number of boundary segments in the x_1 and x_2 directions, respectively. In this study, initial values of L_1 and L_2 are set to 1.0. A nodal point is described by its initial position (X_1, X_2) and by $x_1(X_1,X_2)$ and $x_2(X_1,X_2)$ in its deformed configuration.

The L_1L_2 sheet is deformed by applying prescribed displacements at the edges

$$x_1(0,X_2) = -u_1/2, \quad x_1(L_1,X_2) = L_1 + u_1/2, \tag{11}$$

$$x_2(X_1,0) = -u_2/2, \quad x_2(X_1,L_2) = L_2 + u_2/2. \tag{12}$$

3. Numerical computation of a spring network

The tension-strain relationship of 2D spring sheets is computed numerically for uniaxial and isotropic deformation. Although we are only interested in the steady state, it is numerically convenient to have a time-dependent term in the momentum equation, so that one can use an explicit time-marching scheme. The momentum equation at each node may be modified as the balance between an artificial damping force and the spring forces

$$\kappa \boldsymbol{v}_i = \sum_j \boldsymbol{f}_{ij} = \boldsymbol{F}_i, \tag{13}$$

where κ is the artificial damping coefficient and $\boldsymbol{v}_i$ is the velocity of node i. The viscous term has no physical meaning and generates no force when the system reaches the steady state. Using an Euler explicit scheme, the above equation can be discretized as

$$\boldsymbol{r}_i(t+\Delta t) = \boldsymbol{r}_i(t) + \frac{\Delta t}{\kappa}\boldsymbol{F}_i(t), \tag{14}$$

where Δt is the time step. The convergence of the numerical simulation is defined by

$$\max\left[\frac{\boldsymbol{r}_i(t+\Delta t) - \boldsymbol{r}_i(t)}{\Delta t}\right] \leqslant 10^{-12}. \tag{15}$$

The boundary conditions are those provided by Eqs. (11) and (12) with $u_2 = 0$ for uniaxial deformation and $u_1 = u_2 = u$ for isotropic deformation. Once the deformation reaches a stable state, it is easy to calculate the principal extension ratios λ_1 and λ_2 and the relative area change $\Delta S/S_0$.

C. Relation between spring network and continuum models

We analyze the mechanical properties of the discrete spring network model within the context of continuum models. The boundary conditions (11) and (12) imposed on the

discrete model correspond to $\lambda_1 = (L_1 + u_1)/L_1$ and $\lambda_2 = (L_2 + u_2)/L_2$. The tensions on the edges are computed as

$$T_1 = \frac{\sum_i F_{i,1}|_{x_1=-u_1/2}}{\lambda_2 L_2}, \quad T_2 = \frac{\sum_j F_{j,2}|_{x_2=-u_2/2}}{\lambda_1 L_1}, \tag{16}$$

where $F_{i,1}$ represents the x_1 component of the total spring force $\boldsymbol{F}_i$ acting on node i and $F_{j,2}$ its x_2 component. In the limit of small deformation the relation between tensions and deformation yields the values of G_s and ν_s as a function of k.

III. DEFORMATION OF A 2D SPRING SHEET

We first investigate the deformation of a 2D material under uniaxial or isotropic extension. We derive analytically the Poisson ratio, Young modulus, and area dilation modulus of a spring network model in the small deformation limit and we compare those parameters with their values for continuum constitutive laws. We then compare numerically the stress-strain relationship between the discrete spring network and continuum models in large deformation.

A. Analytical solution for infinitely fine mesh in the small deformation limit

We consider an infinitely fine spring network and derive the relation between force and deformation for a single inner mesh (i.e., far from the edges), assuming that all the mesh elements are identically deformed so that the forces acting on the nodes are symmetric. For the sake of simplicity, we only detail here the derivation of the elastic constant for a cross mesh element; the material properties can be similarly derived for other mesh types using the same procedure.

The springs numbering is shown in Fig. 3. Spring 1 is orientated in the x_1 direction, spring 2 in the x_2 direction, and spring 3 along the cross direction. The initial angle between springs 1 and 3 is θ_0. Let the initial length of springs 1, 2, and 3 be, respectively, l_0, w_0, and $L_0 = (l_0^2 + w_0^2)^{1/2}$.

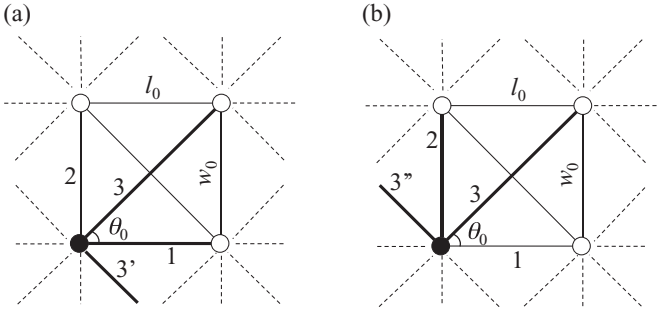

FIG. 3. Numbering of the springs that are taken into account to calculate the forces acting on a node for homogeneous mesh deformation: (a) Springs 1, 3, and 3″ contribute to the x_1-force component; (b) springs 2, 3, and 3″ contribute to the x_2-force component. Springs 3′ and 3″ are the counterparts of spring 3, generated by the periodic boundary condition. The initial lengths are l_0 for spring 1 and w_0 for spring 2. The initial length of springs 3, 3′, and 3″ is $L_0 = \sqrt{l_0^2 + w_0^2}$. The initial angle between springs 1 and 3 is θ_0.

The spring network is deformed from l_0 to $l_0 + \Delta l$ ($|\Delta l| \ll l_0$) in the x_1 direction and from w_0 to $w_0 + \Delta w$ ($|\Delta w| \ll w_0$) in the x_2 direction. We also have

$$(L_0 + \Delta L)^2 = (l_0 + \Delta l)^2 + (w_0 + \Delta w)^2, \tag{17}$$

where ΔL is the length change of spring 3. In the small deformation limit, after neglecting the second-order terms, Eq. (17) is simplified

$$\Delta L = \frac{l_0 \Delta l + w_0 \Delta w}{L_0}. \tag{18}$$

For homogeneous deformation, the components of total spring force F acting at the nodal point is due to springs 1, 3, and 3″ in the x_1 direction and to springs 2, 3, and 3″ in the x_2 direction (Fig. 3)

$$F_1 = k\Delta l + 2k\Delta L \cos(\theta_0 + \Delta\theta), \tag{19}$$

$$F_2 = k\Delta w + 2k\Delta L \sin(\theta_0 + \Delta\theta), \tag{20}$$

where $\Delta\theta$ is the angle change. The local tensions T_1 and T_2 on a mesh are given by

$$T_1 = \frac{F_1}{w_0 + \Delta w}, \quad T_2 = \frac{F_2}{l_0 + \Delta l}. \tag{21}$$

1. *Uniaxial and isotropic deformation*

The spring network is first stretched in the x_1 direction under an external tension T_1, while $T_2 = 0$. The transverse displacement Δw can be deduced from Eq. (20)

$$\Delta w/\Delta l = -\frac{2l_0 \sin\theta_0}{L_0 + 2w_0 \sin\theta_0}. \tag{22}$$

In the small deformation limit, the Poisson ratio is thus given by

$$\nu_s = \frac{|\Delta w/w_0|}{\Delta l/l_0} = \frac{2l_0 \sin\theta_0}{L_0 + 2w_0 \sin\theta_0}\frac{l_0}{w_0}. \tag{23}$$

Substituting Eq. (22) into Eq. (19), we obtain the expression of F_1 as a function of Δl, from which the small deformation Young modulus follows

$$E_s = \frac{T_1}{\Delta l/l_0} = \frac{L_0 + 2w_0 \sin\theta_0 + 2l_0 \cos\theta_0}{L_0 + 2w_0 \sin\theta_0}\frac{l_0}{w_0}k. \tag{24}$$

In another experiment, the spring network is stretched in the x_1 and x_2 directions by an isotropic tension $T_1 = T_2 = T$. Using Eqs. (19) to (21), we find for small deformation

$$\frac{\Delta w}{\Delta l} = \frac{L_0 l_0 + 2l_0^2 \cos\theta_0 - 2l_0 w_0 \sin\theta_0}{L_0 w_0 + 2w_0^2 \sin\theta_0 - 2l_0 w_0 \cos\theta_0}, \tag{25}$$

$$\Delta S/S = \Delta w/w_0 + \Delta l/l_0. \tag{26}$$

The tension T is deduced from Eq. (21)

$$T = 2\frac{L_0 + w_0 \sin\theta_0 + l_0 \cos\theta_0}{L_0 + w_0 \sin\theta_0 - l_0 \cos\theta_0}\frac{\Delta l}{w_0}k. \tag{27}$$

Thus, the area dilation modulus K_s is

$$K_s = \frac{T}{\Delta S/S} = \frac{l_0 w_0 (L_0 + 2w_0 \sin\theta_0 + 2l_0 \cos\theta_0)}{L_0^3 + 2l_0^3 \cos\theta_0 + 2w_0^3 \sin\theta_0 - 2l_0 w_0 (l_0 \sin\theta_0 + w_0 \cos\theta_0)} k. \tag{28}$$

2. *Influence of mesh topology*

The small deformation analytical expressions of Young modulus E_s, Poisson ratio ν_s, and area dilation modulus K_s are given in Tables I and II for cross, cross-center, and regular triangle meshes undergoing homogeneous deformation. A number of conclusions can be drawn.

(1) A nonisotropic mesh ($l_0 \neq w_0$) leads to anisotropic elastic properties for the membrane. It can be easily checked that the values of E_s and ν_s would be different from Eqs. (24) and (23) if the uniaxial stretching were applied along the x_2 direction rather that the x_1 direction.

(2) An isotropic membrane must therefore be modeled with an isotropic mesh ($l_0 = w_0, \theta_0 = \pi/4$ for cross and cross center).

(3) Even for an isotropic mesh, the Poisson ratio depends on the mesh geometry, as is apparent from Table I. The Young modulus, and thus the shear modulus G_s, also depend on the mesh geometry and are proportional to the spring constant.

B. Effect of mesh size

To investigate the influence of the mesh resolution in the small deformation limit, we compute numerically the ratio between the spring constant and the elastic properties for isotropic meshes with different grid spacing, $l_0 = \Delta L$, ranging from 0.003 to 1.0. We follow the numerical method explained in Sec. II B and apply it to cross, cross-center, and unstructured meshes.

Figure 4 shows the values of k/E_s and of k/K_s as functions of mesh size, obtained for the three networks. It is clear that the geometry and size of the mesh have an influence on the results. This is due to the fact that, when the mesh is coarse, the hypothesis of a homogenous deformation of the individual meshes becomes incorrect (a direct consequence of the Saint-Venant principle). There is then a significant influence of the boundary conditions at the sample edges.

For cross and cross-center settings, as the mesh is refined, the values of k/E_s and of k/K_s converge toward the analytical values for homogeneous isotropic meshes given in Tables I and II. The deviation from the analytical value is less than 1% when $\Delta L < 0.025$. The Poisson ratio, inferred from k/E_s and of k/K_s, is also in good agreement with the analytical values. The case $\Delta L = 1$ corresponds to a single mesh. For a cross and cross-center mesh, k/E_s is then equal to 0.375 and 0.417, respectively. These values are obtained by following the method of Sec. III A and applying a nonsymmetric boundary condition.

Mesh convergence is also found for the unstructured mesh. For $\Delta L = 0.005$, the maximum relative variation for k/E_s or k/K_s is less than 0.1%. However, the converged values of k/E_s and of k/K_s for the unstructured mesh are smaller than the analytical solution for the regular triangle. Both meshes would still be expected to behave similarly, as they are both constructed with triangle meshes, each node being connected to six springs. The difference in the spring constant between the regular triangle and unstructured meshes is therefore likely to be due to the random departure from the exact isotropy of the unstructured mesh. The Poisson ratio, however, is equal to 1/3 as predicted for the regular triangular mesh. Similar results have been reached by Hansen *et al.* [22] who showed that the detailed geometry of an unstructured triangular mesh had an influence on the bulk elastic properties of the sheet.

TABLE I. Relationship between the spring constant k, Young modulus E_s, and Poisson ratio ν_s in the small deformation limit for a 2D material under uniaxial deformation. The material is discretized by three types of meshes and subjected to homogeneous deformation. The arrows indicate the directions of extension.

Mesh Type	k as a function of E_s	ν_s
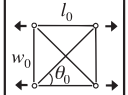	$k = \frac{L_0 + 2w_0 \sin\theta_0}{L_0 + 2(w_0 \sin\theta_0 + l_0 \cos\theta_0)} \frac{w_0}{l_0} E_s$ Isotropic mesh: $k = 2/3\ E_s$	$\nu_s = \frac{2l_0 \sin\theta_0}{L_0 + 2w_0 \sin\theta_0} \frac{l_0}{w_0}$ Isotropic mesh: $\nu_s = 1/2$
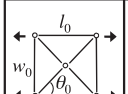	$k = \frac{L_0 + w_0 \sin\theta_0}{L_0 + w_0 \sin\theta_0 + l_0 \cos\theta_0} \frac{w_0}{l_0} E_s$ Isotropic mesh: $k = 3/4\ E_s$	$\nu_s = \frac{l_0 \sin\theta_0}{L_0 + w_0 \sin\theta_0} \frac{l_0}{w_0}$ Isotropic mesh: $\nu_s = 1/3$
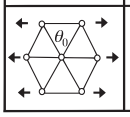	Isotropic mesh: $k = \frac{\sqrt{3}}{2} E_s$	Isotropic mesh: $\nu_s = 1/3$

TABLE II. Relationship between the spring constant k and area dilation modulus K_s in the small deformation limit for a 2D material under isotropic deformation. The material is discretized by three types of meshes and subjected to homogeneous deformation. The arrows indicate the directions of extension.

Mesh Type	k as a function of K_s
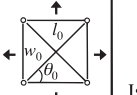	$k = \frac{L_0^3 + 2l_0^3 \cos\theta_0 + 2w_0^3 \sin\theta_0 - 2l_0 w_0 (l_0 \sin\theta_0 + w_0 \cos\theta_0)}{l_0 w_0 (L_0 + 2w_0 \sin\theta_0 + 2l_0 \cos\theta_0)} K_s$ Isotropic mesh: $k = 2/3\ K_s$
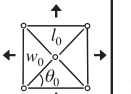	$k = \frac{L_0^3 + l_0^3 \cos\theta_0 + w_0^3 \sin\theta_0 - l_0 w_0 (l_0 \sin\theta_0 + w_0 \cos\theta_0)}{l_0 w_0 (L_0 + w_0 \sin\theta_0 + l_0 \cos\theta_0)} K_s$ Isotropic mesh: $k = K_s$
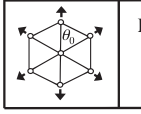	Isotropic mesh: $k = \frac{2}{\sqrt{3}} K_s$

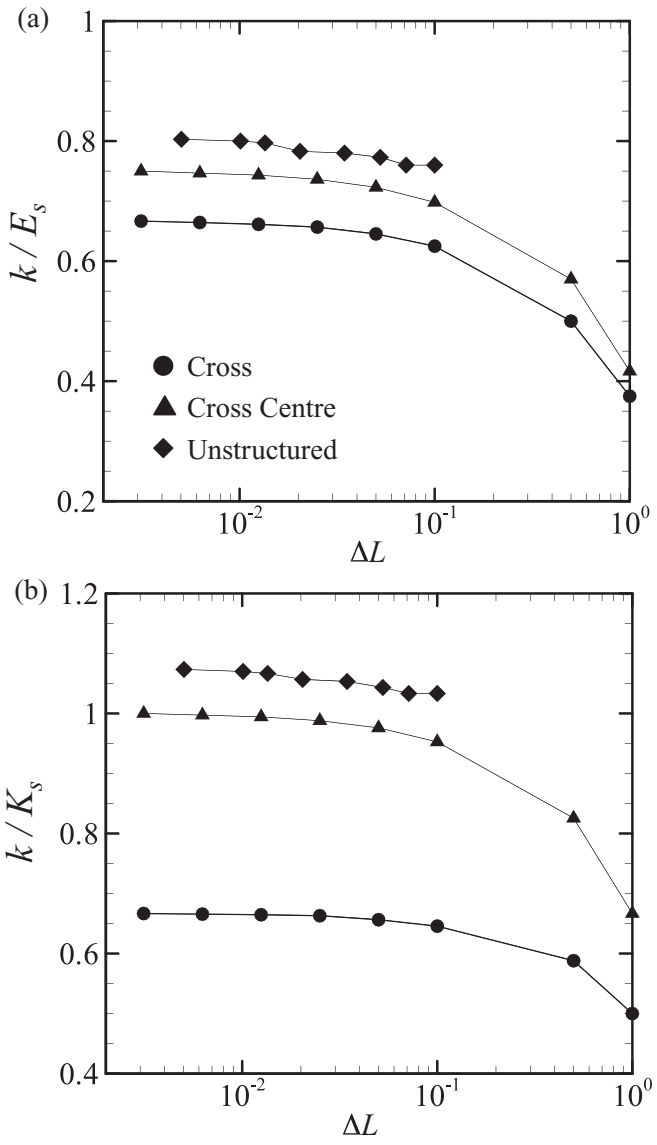

FIG. 4. Spring constants as a function of initial grid spacing for several mesh types under (a) uniaxial extension and (b) isotropic extension. A single mesh corresponds to $\Delta L = 1$. When the mesh is refined, the spring constant converges to the analytical value for an homogeneous network.

C. Comparison of spring network and continuum models

We compare the small deformation mechanical properties of spring network models with an isotropic mesh and the constitutive laws MR and SK. Recall that the Poisson ratio of a spring network is determined by the mesh configuration and is independent of k. For the homogeneous square cross mesh, the Poisson ratio ($\nu_s = 1/2$) is equal to that of a SK ($C = 1$) or MR membrane according to Eqs. (7) and (9). If the spring constant is further set to $k/G_s = 2$, the small deformation mechanical properties E_s, G_s, and K_s of the square cross mesh model are identical to those of a MR or of SK ($C = 1$) membrane. In the case of the square cross-center mesh and the regular triangle mesh with periodic boundary conditions, the Poisson ratio is $1/3$, which corresponds to the Poisson ratio of a SK law with $C = 1/2$. By adjusting $k/G_s = 2$ for the cross-center mesh and $k/G_s = 4/\sqrt{3}$ for the regular-triangle mesh, the mechanical properties of the spring network models coincides with these of a SK ($C = 1/2$) law. It is not possible to match the mechanical properties of a square cross-center model with those of an MR membrane.

D. Large deformation

We now compare numerically the tension-strain relationships of a spring network discretized with square cross, cross-center, and unstructured meshes and a continuum model under *large* uniaxial and isotropic deformation. In all cases, we use a small enough mesh to ensure a constant ratio between k and G_s ($\Delta L = 0.003$ for the cross and cross-center mesh and $\Delta L = 0.005$ for the unstructured mesh).

The tension-strain relationships are shown in Fig. 5(a) for several membrane models under large uniaxial elongation. We note that SK law is strain hardening while MR law is strain softening, as mentioned earlier. The cross mesh model exhibits a strain-hardening behavior similar to SK law. However, the cross-center and unstructured meshes have a quasilinear tension-strain relationship, similar to Hooke's law, even for large deformation.

The isotropic tension-area dilation relations are shown in Fig. 5(b). All three spring network models are strain softening. This can be explained by considering the isotropic deformation of a regular triangle with initial length l_0. The initial surface area is $S_0 = \sqrt{3}l_0^2/4$. When all the springs are equally elongated from l_0 to $l_0 + \Delta l$, the deformed surface area is $S = \sqrt{3}(l_0 + \Delta l)^2/4$ and the relative area change is

$$\frac{\Delta S}{S_0} = \frac{S - S_0}{S_0} = \frac{2l_0\Delta l + \Delta l^2}{l_0^2}. \tag{29}$$

As the spring force is given by $f = k\Delta l$, the relative area change becomes

$$\frac{\Delta S}{S_0} = \frac{f^2 + 2l_0kf}{l_0^2k^2}. \tag{30}$$

This equation shows that the relationship between relative area change and spring force is quadratic, yielding a strain-softening behavior. In a similar manner, the same strain-softening behavior can be predicted for square-mesh cases.

When modeling biological cell membranes, such as a red-blood-cell membrane, local area dilation resistance has to be enforced. In the spring network model, the membrane always shows a strain-softening behavior and imposing the local area incompressibility is impossible. Thus a simple spring model does not seem appropriate to simulate the behavior of an area incompressible biological cell membrane.

IV. INFLATION OF A CAPSULE

When a spherical capsule is inflated by a radial pressure difference between the inside and outside of the membrane, its membrane is under in-plane traction. In this section, we are interested in checking whether the curved surface of the capsule influences the conclusions found for a flat 2D membrane in Sec. III.

It has been observed earlier that the grid of the spring network model must be isotropic to reproduce isotropic

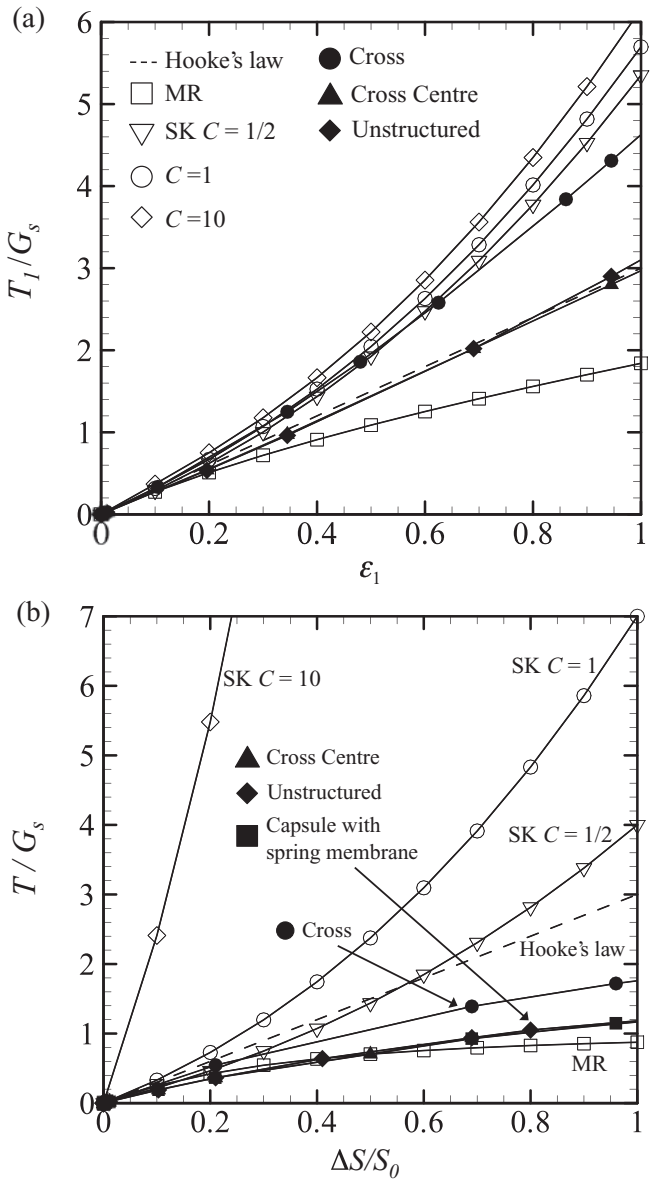

FIG. 5. Tension-strain relationship under (a) uniaxial elongation and (b) isotropic dilation for continuum and spring models.

material properties. It is, however, impossible to generate an isotropic mesh on a spherical surface such as the membrane of a capsule. The most regular mesh that may be generated for a sphere is a regular icosahedron. The triangles of the icosahedron are successively divided into four triangles and the new nodes are projected onto the sphere at each step. The process is repeated until the desired mesh size is obtained. In this study, the membrane is discretized with 1280 triangle elements.

We set as boundary condition a uniform stretched radius $R = R_0 + \Delta R$, where R_0 is the initial radius of the capsule and ΔR is the radius change. The positions of all the nodal points are therefore fixed. For the continuous-membrane model, the tension T in the membrane can be calculated by the Laplace equation $T = R\Delta P/2$, where ΔP is the pressure jump between the inner and outer sides of the membrane. In the case of the discrete spring model, we assume the equilibrium between the average pressure jump across the membrane and the component of the spring force normal to the membrane. We thus define the tension T as

$$T = -\frac{R^{\text{ave}}}{2S}\sum_i \boldsymbol{F}_i \boldsymbol{n}_i, \tag{31}$$

where R^{ave} is the average radius of the capsule and $\boldsymbol{n}_i$ is the outward normal unit vector to the surface at node i. The surface area S of the discrete spring model is calculated by summing the surface areas of all the triangles.

The spring constant of the capsule membrane is adjusted, so that it coincides, in the small deformation limit, with the value of K_s/G_s of the SK law with $C = 1/2$. The tension-strain curve can be perfectly superimposed onto the results found under 2D isotropic deformation with the cross-center and unstructured meshes. Mesh refinement has not been seen to have an effect on the results, indicating that the mesh convergence is reached. From these results, we conclude that, for isotropic extensions, previous findings on the mechanical properties of flat 2D spring sheet can be applied to curved surface membranes and therefore to the study of capsule inflation.

V. CAPSULE IN SIMPLE SHEAR FLOW

In many real situations, the length scale of the outer flow field is often much larger than the capsule size. In such cases, flow around the capsules can be linearized. Thus we investigate the deformation of a spherical capsule in a simple shear flow which is a typical example of a linear shear flow.

Consider the capsule is freely suspended in a Newtonian fluid with the same viscosity μ and density as the internal Newtonian fluid. With respect to axes centered on the capsule center, the undisturbed flow velocity field $\boldsymbol{v}^\infty$ of the external fluid is given by

$$v_1^\infty = \dot{\gamma} x_2, \quad v_2^\infty = v_3^\infty = 0, \tag{32}$$

where $\dot{\gamma}$ is the shear rate of the external fluid.

One important parameter that governs the deformation of the capsule is the capillary number, which is the ratio between the viscous stress exerted by the fluid and the elastic resistance of the membrane

$$\text{Ca} = \frac{\mu R \dot{\gamma}}{G_s}. \tag{33}$$

For the spring network model, Ca is calculated assuming $k/G_s = 4/\sqrt{3}$, as discussed in Sec. III C. The capillary number varies with capsule size (R), flow strength ($\mu\dot{\gamma}$), and membrane elasticity (G_s). To cover a wide range of physical situations, we vary Ca from 0 to 3.5 and use either MR or SK law for the continuum model. We then discuss the difference between spring network and continuum constitutive laws.

A. Motion of the internal and external liquids

Owing to the small dimensions of the particle, the particle Reynolds number is very small and the Stokes equations apply for both the internal and external fluid motion. Under this

assumption, the velocity field $\boldsymbol{v}$ at any point $\boldsymbol{x}$ is given by the well-known integral formulation [4]

$$\boldsymbol{v}(\boldsymbol{x}) = \boldsymbol{v}^{\infty}(\boldsymbol{x}) - \frac{1}{8\pi\mu}\int_S \boldsymbol{J}(\boldsymbol{x},\boldsymbol{y})\boldsymbol{q}(\boldsymbol{y})dS, \tag{34}$$

where $\boldsymbol{v}^{\infty}$ is the undisturbed velocity field and $\boldsymbol{q}$ is the force per unit area exerted by the membrane on the fluids, $\boldsymbol{J}$ is the Green's function of the single-layer potential defined by

$$J_{ij}(\boldsymbol{x},\boldsymbol{y}) = \frac{\delta_{ij}}{r} + \frac{r_i r_j}{r^3}, \tag{35}$$

with $\boldsymbol{r} = \boldsymbol{y} - \boldsymbol{x}$ and $r = |\boldsymbol{r}|$.

B. Membrane mechanics with spring network

When we solve the membrane equation with a spring network model, the spring forces are calculated by Eq. (10). The load $\boldsymbol{q}$ in Eq. (34) is computed at each node i

$$\boldsymbol{q}_i = \frac{1}{dA_i}\sum_k \boldsymbol{f}_{i,k}, \tag{36}$$

where the summation is done on all the adjacent nodes and dA_i is the surface area calculated as follows. Let point g_j be the center of gravity of the element e_j, which is surrounding point i. dA_i is calculated by summing up triangles $da_{j,j+1}$ made by the points i, g_j, g_{j+1}

$$dA_i = \sum_j^{n_i} da_{j,j+1}, \tag{37}$$

where n_i is the number of elements connected to node i.

C. Numerical method

Equation (34) is solved with a boundary-element method following the method by Lac *et al.* [2,3]. A structured quadrilateral grid based on spherical coordinates is used and the different quantities are interpolated with bicubic B-spline functions. The presence of poles connected to multiple nodes leads to a singularity for the solid mechanics problem, which is then solved on an unstructured triangular mesh. We therefore use an interpolation scheme to transfer the physical quantities between the triangular mesh used for the solid problem [Fig. 6(b)] and the quadrilateral mesh used in fluid problem [Fig. 6(a)]. In this study, we use a first-order interpolation. Any quantity of the quadrilateral mesh can be projected onto the triangular mesh. Let point i be in the triangle defined by the nodes i_1, i_2, i_3 [Figure 6(c)]. A function f at point i takes the value $f(i) = A_{23}f(i_1) + A_{31}f(i_2) + A_{12}f(i_3)$, where $A_{\alpha\beta}$ is the ratio of the triangle surface area made by points i, i_α, and i_β to the triangle surface area made by points i_1, i_2, and i_3. In a similar manner, physical quantities on the triangular mesh can be interpolated using those on the quadrilateral mesh.

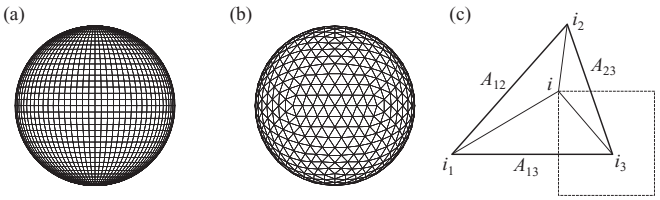

FIG. 6. (a) Quadrilateral mesh used in fluid solver and (b) triangular mesh used in solid solver. (c) To transfer physical quantities between the two, we use a first-order interpolation. Example of a nodal point i of the quadrilateral mesh that is projected onto the triangular mesh.

At any given time t, we know the displacement of the membrane, so that the load $\boldsymbol{q}$ on the membrane can be calculated. The integral equation yields the new velocity field and the membrane positions are updated using an explicit fourth-order Runge-Kutta method.

The nondimensional time step $\dot{\gamma}\Delta t$ is set at 0.005 and the procedure is stopped when the dimensionless time $\dot{\gamma}t$ is equal to 20, which is larger than two times the time needed for the deformation of the capsule to reach the steady state.

The steady-state three-dimensional deformation of the capsule can be measured using the Taylor parameter

$$D_{ij}^{\infty} = \frac{|b_i - b_j|}{b_i + b_j}, \quad \text{for} \quad i,j = 1,2,3, \tag{38}$$

where b_1, b_2, and b_3 denote the three semi-axis lengths of the ellipsoid of inertia of the deformed capsule, used to estimate the capsule deformation [14].

The mesh convergence is verified by changing the mesh size. We have considered a discretization of the membrane with 1280 triangle elements for the solid solver and 3200 quadrilateral elements for the fluid solver as well as a refined mesh with 5120 triangular and 5000 quadrilateral elements. The maximum change in the Taylor parameter between the two cases is less than 1%. Since the Taylor parameter has converged for the mesh with 1280 triangular and 3200 quadrilateral elements, we will consider these mesh elements hereafter.

D. Deformation of a capsule in a simple shear flow

Figure 7 shows the Taylor parameter as a function of Ca for capsules with MR and SK membrane (Lac *et al.* results [2]),

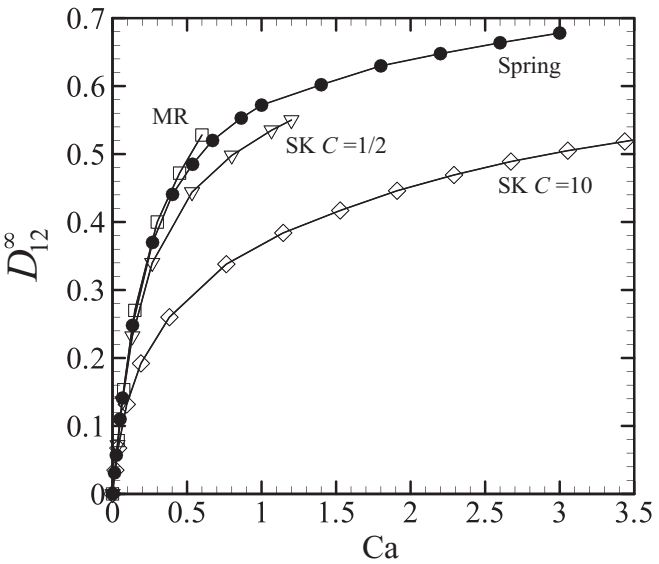

FIG. 7. Evolution of the Taylor deformation in the shear plane, with the capillary number Ca for capsules with MR, SK, and spring network membranes.

as well as with a spring network membrane. For a capsule subjected to strong flow (large Ca), the deformation of a capsule enclosed by a spring network is larger than that of a capsule enclosed with a SK $C = 1/2$ membrane, although the two membranes have the same mechanical properties in the small deformation limit. This is due to the fact that the spring network is strain softening under large deformation, whereas the SK $C = 1/2$ membrane is strain hardening.

However, since the bending rigidity of the membrane has been neglected, the membrane is mechanically stable only if it is under tension everywhere. The study of the sign of the principal tension T in the membrane provides a way to evaluate the stability of the equilibrium state which is computed: If the minimum value $T_{\min}$ is negative, the membrane is under compression somewhere on its surface and the equilibrium is unstable. Lac *et al.* [2] and Walter *et al.* [30] found that the membrane is under tension and thus mechanically stable for a limited range of capillary numbers where $T_{\min} > 0$. We denote $\mathrm{Ca_L}$ and $\mathrm{Ca_H}$ the two critical capillary numbers defined by $T_{\min}(\mathrm{Ca}_L) = T_{\min}(\mathrm{Ca}_H) = 0, \mathrm{Ca}_L \leqslant \mathrm{Ca}_H$. When $\mathrm{Ca} < \mathrm{Ca}_L$, the initially spherical capsule is extended by the flow in the principal straining direction (oriented at $\pi/4$ with respect to the streamlines). The capsule being a closed shape with a constant volume, it is thus compressed along the equator and tends to buckle in this area. When $\mathrm{Ca} > \mathrm{Ca}_H$, the compression zone appears near the tip of the capsule and is due to the high curvature of this region.

We also observe low-shear (in the equator area) and high-shear (near the tips) oscillations of the normal load using a spring network as shown in Fig. 8. Such oscillations indicate a tendency toward buckling. As it is impossible to compute principal tensions in the case of a discrete spring network

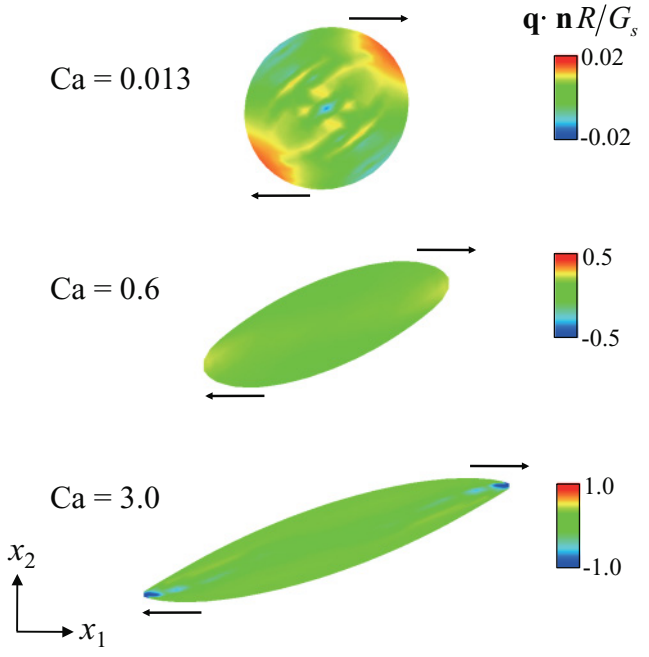

FIG. 8. (Color) Deformation of the capsule with a spring network model under $\mathrm{Ca} = 0.013, 0.6, 3.0$. The background shear is applied in the x_1-x_2 plane, where x_1 is taken in the flow direction. The color scale represents the normal component of the load.

model, we have determined limits Ca'_L and Ca'_H on the basis of the sign of the normal component of surface load by means of the conditions $\boldsymbol{q}(\mathrm{Ca}'_L)\boldsymbol{n} = \boldsymbol{q}(\mathrm{Ca}'_H)\boldsymbol{n} = 0$, $\mathrm{Ca}'_L \leqslant \mathrm{Ca}'_H$. This condition is less stringent that the one on the negative principal tensions, as the membrane may be under compression, but not oscillate because of numerical stiffness. As a result we find

$$\mathrm{Ca}'_L = 0.3, \quad \mathrm{Ca}'_H = 1.0,$$

whereas Lac *et al.* [2] found a smaller range of stability for a Sk law with $C = 0.5$

$$\mathrm{Ca}'_L = 0.8, \quad \mathrm{Ca}'_H = 1.2.$$

Although the two criteria are different, they provide a stability range which is roughly of the same order of magnitude.

The occurrence of negative principal tensions with a continuum membrane model or of normal load oscillations with a spring network, all denote that the membrane is undergoing compression and thus might buckle. This phenomenon is controlled by the bending resistance of the membrane. Here, we have not included any bending stiffness in the membrane model and as a consequence we cannot model the actual buckling. However, the membrane has some numerical stiffness that prevents it from collapsing and allows us to compute the motion of a capsule even when compression occurs. Since the aim of this study is to compare the discrete spring network model and 2D in-plane constitutive laws, we do not discuss any further the effect of the bending stiffness on the deformation of the capsule in this paper.

E. Comparison with experiments

Deformation of an artificial capsule in a simple shear flow was investigated experimentally [31,32]. In the work of Chang *et al.* [31], the capsule had a nylon membrane, was filled with a silicon oil, and was suspended in polybutene. The viscosity ratio of the internal to external liquids λ was about 0.004. In the work of Walter *et al.* [32] the capsule membrane was made from polyamid (4-Aminomethyl-1,8-diaminooctane) and the viscosity ratio λ was 0.001. In those two experimental studies, the membrane Young modulus E_s was measured. To compare the experimental and numerical results, a capillary number Ca_{E_s} is defined based on the Young modulus as $\mathrm{Ca}_{E_s} = \mathrm{Ca}G_s/E_s$.

To have similar λ values with the experiments, λ is set as 0.002 in the numerical simulations. In the case of the nonidentical viscosity ratio (i.e., $\lambda \neq 1$) Eq. (34) has to be modified as follows:

$$\boldsymbol{v} = \frac{2}{1+\lambda}\boldsymbol{v}^{\infty} - \frac{1}{4\pi\mu(1+\lambda)}\int_S \boldsymbol{J}\boldsymbol{q}dS + \frac{1}{4\pi}\frac{1-\lambda}{1+\lambda}\int_S \boldsymbol{v}\boldsymbol{K}\boldsymbol{n}dS, \tag{39}$$

where the Green's double layer potential $K_{ijk} = -6(r_i r_j r_k)/r^5$ is introduced. Equation (39) is solved by the boundary element method as explained in Ref. [33].

The Taylor parameter is shown as a function of capillary number in Fig. 9. The behavior of SK $C = 1$ is similar to the nylon capsule (indicated as "Chang *et al.*" in Fig. 9) in a wide range of capillary numbers. In the case of the

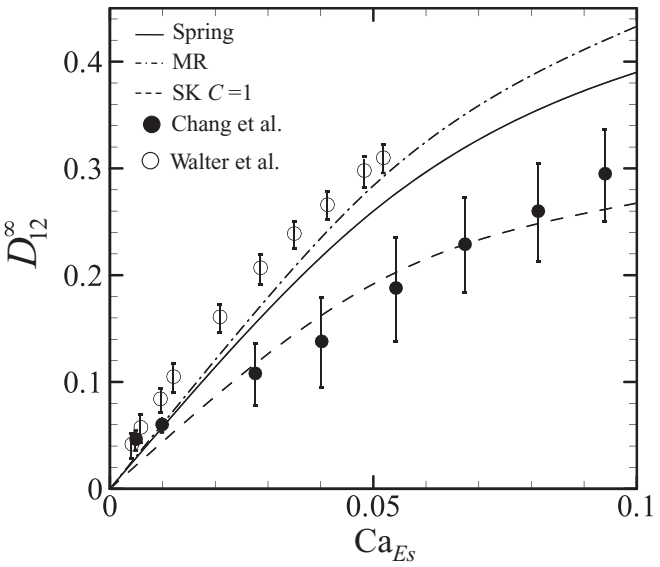

FIG. 9. Taylor parameter as a function of capillary number Ca_{E_s}. Ca_{E_s} is defined by using Young modulus instead of shear modulus. Viscosity ratio between internal and external liquids is set as $\lambda = 0.002$ in the numerical models, whereas $\lambda \approx 0.004$ and 0.001 in the paper of Chang *et al.* and Walter *et al.*, respectively. (Note the error bars for the two experimental results do not represent standard deviations but the maximum and minimum values in the experiments.)

polyamid capsule ("Walter *et al.*" in the figure), the Taylor parameter has higher values than those of the nylon capsule. By employing a proper continuum model with an appropriate model parameter, the experimental results can be well captured. In the case of the simple spring model, it is difficult to express various experimental results by adjusting the spring constant. Thus, continuum models have broader applicability to actual experimental situations.

VI. CONCLUSION

In this study, we have compared the mechanical properties of a membrane modeled with continuum constitutive laws and a discrete spring network under various conditions: uniaxial and isotropic deformations of a 2D membrane, inflation of a capsule, and deformation of an initially spherical capsule in a simple shear flow. The results have shown that the mechanical properties of spring networks are strongly dependent on the mesh configuration.

In the small deformation limit, the mechanical properties of the spring network model may be predicted analytically. It is found that the spring network model has anisotropic mechanical properties, in general. However, isotropic meshes have mechanical properties that converge toward those of an isotropic material. To express isotropic elasticity using a spring network model, the mesh must therefore be isotropic and sufficiently fine, relative to the variation of the stress field. Moreover, in the small deformation limit, we observe that the behavior of the spring network with a fine square cross mesh is similar to MR and SK $C = 1$, ($E_s = 3.0G_s$, $\nu_s = 1/2$), by adjusting $k/G_s = 2.0$. The square cross-center and regular-triangle meshes are similar to SK $C = 1/2$ ($E_s = 8/3G_s$, $\nu_s = 1/3$) by adjusting $k/G_s = 2.0$ and $k/G_s = 4/\sqrt{3}$, respectively. These correlations are important because one can determine the spring constant by performing conventional mechanical experiments.

In large deformation, the stress-strain relationship under isotropic elongation shows a strain-softening behavior for all mesh types and it is difficult to express the area-incompressible property. For a capsule in a simple shear flow, we also confirm that a spring network cannot express the D_{12}^{∞}-Ca correlation of a capsule with an area-incompressible membrane. Thus, to express a biological cell membrane, we need to choose a membrane model that can express the local area incompressibility, such as the SK law, instead of a spring network model.

[1] D. Barthès-Biesel, T. Yamaguchi, T. Ishikawa, and E. Lac, J. Biomech. Sci. Eng. **1**, 51 (2006).
[2] E. Lac, D. Barthès-Biesel, N. A. Pelekasis, and J. Tsamopoulos, J. Fluid Mech. **516**, 303 (2004).
[3] E. Lac and D. Barthès-Biesel, Phys. Fluids **17**, 072105 (2005).
[4] C. Pozrikidis, *Boundary Integral and Singularity Methods for Linearized Viscous Flow* (Cambridge University Press, Cambridge, England, 1992).
[5] C. D. Eggleton and A. S. Popel, Phys. Fluids **10**, 1834 (1998).
[6] X. Li and K. Sarkar, J. Comput. Phys. **227**, 4998 (2008).
[7] Y. Sui, Y. T. Chew, P. Roy, Y. P. Cheng, and H. T. Low, Phys. Fluids **20**, 112106 (2008).
[8] Y. Sui, Y. T. Chew, P. Roy, and H. T. Low, J. Comput. Phys. **227**, 6351 (2008).
[9] R. Skalak, A. Tozeren, R. P. Zarda, and S. Chien, Biophys. J. **13**, 245 (1973).
[10] M. Carin, D. Barthès-Biesel, F. Edwards-Lévy, C. Postel, and D. Andrei, Biotechnol. Bioeng. **82**, 207 (2003).
[11] S. Kessler, R. Finken, and U. Seifert, J. Fluid Mech. **605**, 207 (2008).
[12] C. Pozrikidis, J. Fluid Mech. **297**, 123 (1995).
[13] C. Pozrikidis, Ann. Biomed. Eng. **31**, 1194 (2003).
[14] S. Ramanujan and C. Pozrikidis, J. Fluid Mech. **361**, 117 (1998).
[15] A. Diaz and D. Barthès-Biesel, Comput. Model. Eng. Sci. **3**, 321 (2002).
[16] S. K. Doddi and P. Bagchi, Int. J. Multiphase Flow **34**, 966 (2008).
[17] S. K. Doddi and P. Bagchi, Phys. Rev. E **79**, 046318 (2009).
[18] Y. Lefebvre and D. Barthès-Biesel, J. Fluid Mech. **589**, 157 (2007).
[19] A. Diaz, N. Pelekasis, and D. Batrhès-Biesel, Phys. Fluids **12**, 948 (2000).
[20] W. R. Dodson III and P. Dimitrakopoulos, J. Fluid Mech. **641**, 263 (2009).
[21] S. Kwak and C. Pozrikidis, Phys. Fluids **13**, 1234 (2001).
[22] J. C. Hansen, R. Skalak, S. Chien, and A. Hoger, Biophys. J. **70**, 146 (1996).

[23] Y. Navot, Phys. Fluids **10**, 1819 (1998).
[24] T. W. Pan and T. Wang, Int. J. Numer. Anal. Model **6**, 455 (2009).
[25] T. W. Secomb, B. Styp-Rekowska, and A. R. Pries, Ann. Biomed. Eng. **35**, 755 (2007).
[26] K. Tsubota, S. Wada, and T. Yamaguchi, J. Biomech. Sci. Eng. **1**, 159 (2006).
[27] T. Wang, T. W. Pan, Z. W. Xing, and R. Glowinski, Phys. Rev. E **79**, 041916 (2009).
[28] K. Tsubota and S. Wada, Int. J. Mech. Sci. **52**, 356 (2010).
[29] D. Barthès-Biesel, A. Diaz, and E. Dhenin, J. Fluid Mech. **460**, 211 (2002).
[30] J. Walter, A.-V. Salsac, D. Barthès-Biesel, and P. L. Tallec, Int. J. Numer. Meth. Engn. **83**, 829 (2010).
[31] K. S. Chang and W. L. Olbricht, J. Fluid Mech. **250**, 609 (1993).
[32] A. Walter, H. Rehage, and H. Leonhard, Colloids Surf. A **183-185**, 123 (2001).
[33] E. Foessel, J. Walter, A.-V. Salsac, and D. Barthès-Biesel, J. Fluid Mech. **672**, 477 (2011).